Controls by rheological structure of the lithosphere on the temporal evolution of continental magmatism: Inferences from the Pannonian Basin system

Alexander Koptev [a],[*], Sierd Cloetingh [b], István J. Kovács [c],[d],[e], Taras Gerya [f], Todd A. Ehlers [a]

[a] *University of Tübingen, Department of Geosciences, Tübingen, Germany*
[b] *Utrecht University, Tectonics Research Group, Utrecht, Netherlands*
[c] *MTA EK Lendület Pannon LitH$_2$Oscope Research Group, Budapest, Hungary*
[d] *CSFK Geodetic and Geophysical Institute, Sopron, Hungary*
[e] *Centre for Energy Research, Institute for Energy Security and Environmental Safety, Budapest, Hungary*
[f] *Institute of Geophysics, Department of Earth Sciences, ETH-Zurich, Zurich, Switzerland*

ARTICLE INFO

ABSTRACT

Physical-chemical controls of continental magmatism evolution remain enigmatic. Of prime and controversial nature is the temporal transition from calc-alkaline magmas to alkali basalts, correlated with a switch in tectonic regime from extension to compression. We perform 1D thermo-kinematic modelling to analyze the evolution of the thermo-rheological structure of the lithosphere in such settings using the Northwestern Pannonian Basin as a test-bed. Given well-known evidence for major reduction of brittle deformation parameters due to melt-related softening, we use a relatively low internal angle of friction. We demonstrate that at the termination of extension, the presence of intra-crustal low-viscosity layers in the lithosphere provides optimal condition for emplacement and differentiation of intermediate crustal magmatic chambers along the pathway of deep-sourced basaltic melts. In contrast, subsequent lithosphere cooling after the end of extension combined with tectonic and magmatic thickening lead to a disappearance of the low-viscosity layers and formation of lithospheric-scale faults. The latter serve as conduits for rapid ascent of uncontaminated alkali basaltic melts from the mantle to the surface. These findings shed new light on the geodynamic controls of magmatism in extensional settings.

© 2021 The Authors. Published by Elsevier B.V. This is an open access article under the CC BY-NC-ND license (http://creativecommons.org/licenses/by-nc-nd/4.0/).

1. Introduction

In continental rifts and back-arc extensional systems a transition is often observed from calc-alkaline volcanism during the rifting stage to late-stage alkali basaltic volcanism during post-rift times, such as in the Basin and Range (North America, e.g. Fitton et al., 1991), Eastern Morocco Rift (e.g. El Bakkali et al., 1998), and the Pannonian Basin (Central Europe, e.g. Seghedi et al., 2004; Kovács and Szabó, 2008). Several mechanisms have been proposed to explain this change in magmatism, such as slab detachment during continental collision (Coulon et al., 2002) and continuous subduction (Ferrari, 2004), delamination (Duggen et al., 2005), and plume emplacement (Márquez et al., 1999). However, little attention was paid so far to quantifying the role of changes in large-scale rheological properties of the lithosphere in enabling upper mantle

melts to reach the surface without or with only very limited contamination of the overlying lithosphere.

Although the term is nowadays used in a wider sense, calc-alkaline rocks can be defined as hydrous and more oxidized magmas covering the range from basaltic to rhyolitic compositions in sub-alkaline magma series (e.g. Sheth et al., 2002). Such calc-alkaline magmas originate from subduction-contaminated asthenospheric basaltic melts or lithospheric melts through assimilation, fractionation and crystallization processes at different levels in the lithosphere. Basalts with high alkali content (i.e. alkali basalts) are characterized by the presence of olivine and augite as phenocrysts and normative nepheline (Le Maitre et al., 2005). In contrast to calc-alkaline magmas, alkali basalts can originate directly from the asthenosphere or from the metasomatized lithospheric mantle without or with limited contamination.

Two conditions are critical for near-surface emplacement of uncontaminated primary melts from the upper mantle, which are the presence of partially molten material in the upper mantle and lithospheric-scale rupture zones functioning as conduits for rapid
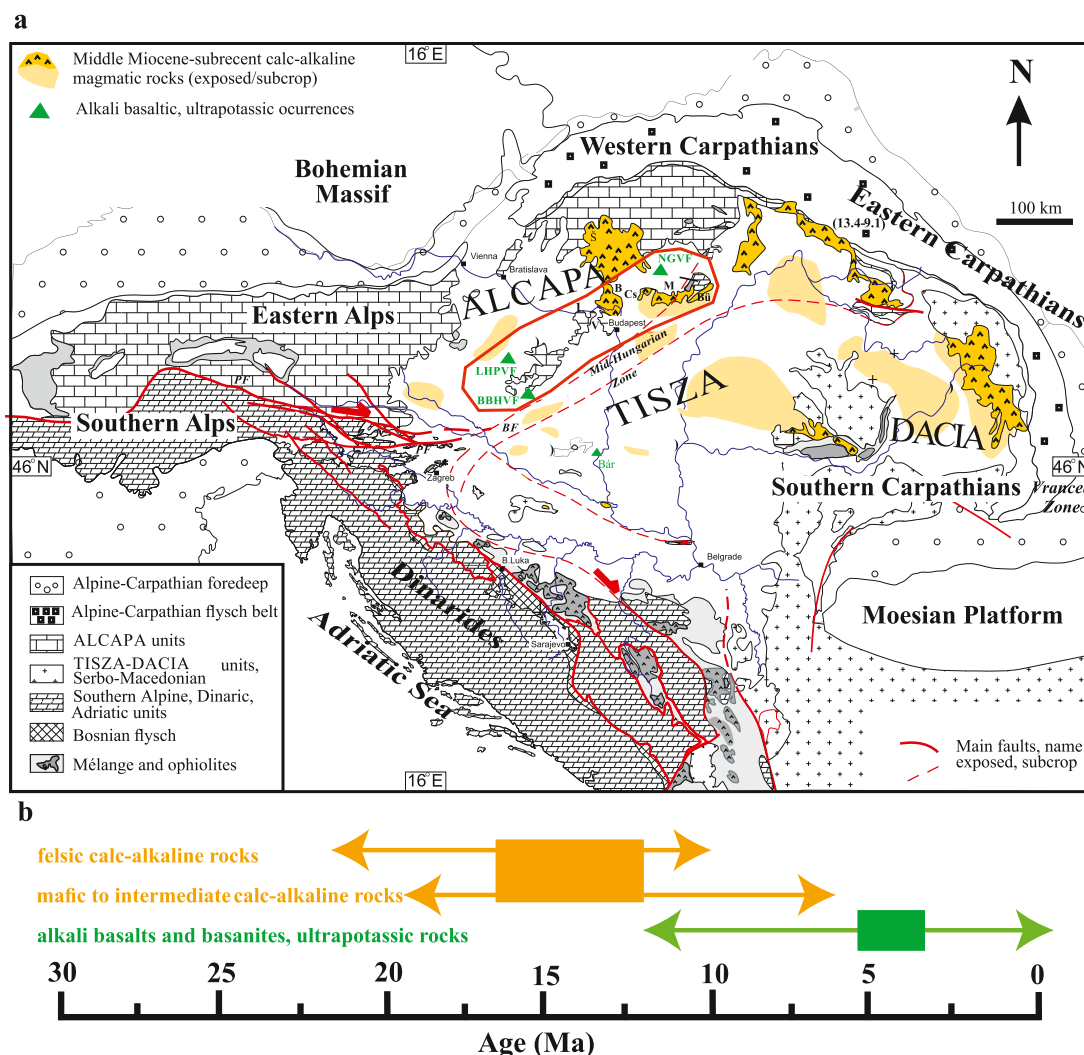
Fig. 1. a) Schematic geological map of the Carpathian-Pannonian region with location of main alkali basaltic localities. The map is modified after Fig. 1. in Kovács et al. (2020). Abbreviations: BBHVF – Bakony-Balaton Highland Volcanic Field; LHPVF – Little Hungarian Plain Volcanic Field; NGVF – Nógrád-Gömör Volcanic Field; PF – Periadriatic fault; BF – Balaton fault; B – Börzsöny; Bü – Bükkalja; Cs – Cserhát; M – Mátra; V – Visegrád. The Northwestern Pannonian Basin system on the ALCAPA unit, the focus area of our study, is encircled by red solid line. b) Major magmatic episodes in the Pannonian Basin system. Double arrowheaded lines show the time span of specific magmatic episodes, whereas rectangles show the main phases of magmatic activities (based on Szakács et al., 2018). (For interpretation of the colours in the figure(s), the reader is referred to the web version of this article.)

transport. Lithospheric-scale faults form preferentially in a rheologically coupled lithosphere when the thicknesses of the crustal ductile layers are significantly reduced (e.g. Ter Voorde et al., 1998; Koptev et al., 2019). Therefore, the examination of this enigmatic feature in the tectono-volcanic evolution requires an analysis of the thermal history and its consequences for the amount of asthenospheric melting. The same is true for assessing its impact on the rheological stratification and degree of mechanical coupling (Koptev et al., 2018; Tetreault and Buiter, 2018) of the overlying lithosphere during and after extension that in turn strongly affects melt transportation and emplacement (Gerya and Burg, 2007).

Here we present the results of a thermo-kinematic study conducted to examine the controls of the thermo-rheological structure of continental lithosphere during extension and subsequent tectonic inversion on the spatial and temporal distribution of intracontinental volcanic activity in terms of its intensity and geochemical signatures. We use the Carpathian-Pannonian orogenic and extensional back-arc system of Central Europe as a natural analogue, constraining lithospheric geometry, composition and polyphase tectonic evolution in our modelling study.

2. The Carpathian-Pannonian system: tectono-magmatic characteristics

The post-Paleogene tectonic evolution of the Carpathian-Pannonian system (Fig. 1a) was mainly driven by the rapid retreat of the Carpathian slab and the associated formation of a large intracontinental extensional back-arc basin starting at around 20-17 Ma (e.g. Horváth et al., 2015). During the slab retreat, the shortening at the exterior of the Carpathians and the Pannonian back-arc extension and lithospheric thinning continued until around 11-9 Ma, when the main subduction plane was locked and extension ceased (e.g. Horváth et al., 2006; Balázs et al., 2016). The extension and the subsequent inversion were heterogeneous in space and time. While in the NW located Alpine-Carpathian-Pannonian (ALCAPA) mega-unit the peak extension took place in the early and middle Miocene, the extension in the SW located Tisza-Dacia part of the basin took place until 9 Ma and generally migrated towards the main depocentres located in the east (Fig. 1a, Matenco and Radivojević, 2012; Balázs et al., 2016). The subsequent evolution of the Carpathians was dominated by slab detachment, steepening and/or delamination leading to the present-day intermediate mantle high-

velocity anomaly and seismicity associated with the Vrancea slab in its SE corner (e.g. Matenco et al., 2007; Petrescu et al., 2021). The Pannonian Basin was inverted in post 9 Ma times by a different process, the indentation of the Adriatic micro-continent on its Dinarides orogenic margin (Fig. 1a) leading to compression and transpression that has started in the SW earlier (from the late Middle Miocene) and gradually migrated towards the east (Fodor et al., 2005; Balázs et al., 2016).

The magmatism of the Carpathian-Pannonian system was also heterogeneous in space and with time. Of particular interest for our study is the magmatism in the NW located ALCAPA mega-unit (the 'Western Segment' of Seghedi et al., 2004), described by numerous previous studies (e.g. Harangi, 2001; Seghedi et al., 2004; Kovács and Szabó, 2008; Seghedi and Downes, 2011). There, a general transition with time from felsic calc-alkaline, mafic to intermediate calc-alkaline, to alkali-basalts, basanite and ultra-potassic rocks was documented (Fig. 1b). Our main aim is to explore possible rheological causes for this shift from calc-alkaline magmatism during the syn-rift phase to alkali basaltic volcanism during the post-rift inversion phase of the Northwestern ALCAPA unit of the Pannonian Basin system and other extensional basins with similar geodynamic history.

Massive calc-alkaline magmatism (Fig. 1b) reflects the mixing of upper mantle magmatic sources with a variable degree of metasomatic or crustal contamination (Seghedi et al., 2004; Kovács and Szabó, 2008; Szakács et al., 2018). In particular, prior subduction phases at the margins of the Pannonian Basin since the Jurassic have pervasively metasomatized the lithosphere and asthenosphere underlying the area (e.g. Schmid et al., 2020). These subduction-related metasomatic fingerprints have been preserved and triggered melting during the subsequent extension stage and their geochemical characteristics are present in both calc-alkaline and alkali basaltic magmas (Harangi, 2001; Kovács and Szabó, 2008). Nevertheless, the contamination, fractionation and crystallisation at various crustal levels played a primary role in the development of calc-alkaline magmas (e.g. Harangi, 2001; Seghedi et al., 2004). On the contrary, extensional decompressional melting of the upwelling asthenosphere can produce almost uncontaminated alkali basaltic melts directly from the upper mantle (Wilson and Downes, 1991; Harangi et al., 2015). In addition, subordinate Middle Miocene syn-rift ultrapotassic and potassic rocks originated from the partial melting of the strongly metasomatized lithospheric mantle. The very small volume Pliocene ultrapotassic magmas in the centre (i.e. Bár) of the Pannonian Basin have (at least partially) asthenospheric origin and show only minor contamination (Harangi, 2001). These latter rocks all show significant enrichment in potassium, which assumes prior metasomatic enrichment of potassium or existence of potassium rich lithologies in their source region (e.g. subducted sediments and recycled crust; Nelson et al., 1986). These very small volume potassic magmas, however, are not in the focus of our study.

In the total alkali silicate (TAS) diagram (Le Maitre et al., 2005) for calc-alkaline and alkali basaltic rocks in the Northwestern Pannonian Basin, alkali basaltic rocks fall in the basaltic, trachy-basalt and tephrite, basanite fields. Calc-alkaline rocks cover a very wide field from basalts to rhyolites. SiO_2 is in the narrow range from 44 to 50 wt.%, whereas total alkalis ($N_2O + K_2O$ wt.%) is between 4-8 wt.% for alkali basaltic rocks. In contrast, calc-alkaline rocks cover a much wider field since the SiO_2 and total alkali content vary from 50 to 77 wt.% and from 0 to 9 wt.% respectively (Fig. 2a).

Calc-alkaline and alkali basaltic rocks are also plotted on the Nb/Y vs. Th/Y diagram (Fig. 2b). The Nb/Y ratio is sensitive to source variation (i.e. geochemical heterogeneity in the source region), whereas the Th/Y ratio is sensitive to source contamination by subduction-related influx of melts/fluids (e.g. Seghedi et al., 2004). Alkali basalts cover only a narrow range in both ratios and

are falling close to the field of ocean island basalts (OIBs, Sun and McDonough, 1989). The compositions of alkali basalts imply only a moderate degree of source variation but no significant source contamination, assimilation, and fractional crystallization. In contrast, calc-alkaline rocks span a much wider range in both ratios referring to appreciable contributions of all factors in explaining the observed geochemical complexity.

A striking observation for the Northwestern Pannonian Basin is the absence of alkali basaltic volcanism at the surface during the syn-rift phase. In contrast, alkali basaltic activity started only ∼11 Ma at the western margin and lasted until subrecent times with the peak of igneous activity clustered around 5-3 Ma (Pécskay et al., 2006; Fig. 1b). This emplacement of alkali basaltic volcanism long after extension times is surprising given that thermal relaxation after the main phase of extension is less favourable for melt generation and preservation in the cooling upper mantle.

A recent study (Kovács et al., 2020) has demonstrated that basaltic partial melts could be present in the cooling asthenosphere at temperatures of 1000-1100 °C when the bulk 'water' content in the mantle is relatively low (a few hundred ppm). This suggests that melts have been transferred from a partially molten asthenosphere to the surface by deep fractures in the overlying lithosphere, inherited or formed by tectonic contraction during thermal relaxation in the post-extensional phase. The end of the syn-rift phase could be an optimal moment for emplacement of deep-sourced mantle melts given the maximum degree of melting and minimum thickness of overlying thinned lithosphere. Therefore, it remains unclear why basaltic partial melts were either retained in the asthenosphere for a long time or were fractionated and/or contaminated in the overlying lithosphere producing calc-alkaline magmas during the syn-rift stage. In addition, an outstanding question is why alkali basalts reached the surface only during tectonic inversion, a tectonic regime generally considered to be less suitable for melt production and extraction.

3. Model description and modelling strategy

To quantify the thermal history of the Northwestern ALCAPA part of the Pannonian Basin system over a 17 Myr period we used a numerical 1D thermo-kinematic model that solves the advection-diffusion equation with radiogenic heat production. In this approach, we link tracking of the time-dependent kinematics of key lithospheric interfaces including the upper/lower crust boundary, Moho, and bottom of the thermal lithosphere (corresponding to an isotherm of 1300 °C) to the thermal evolution calculated with a forward model of thermal diffusion.

In view of the tectonic history of the Northwestern part of the Pannonian Basin (Horváth et al., 2006), the kinematic model prescribes the following three stages including: 1) an extensional phase with thinning of the crust and lithosphere (17-11 Ma); 2) a neutral phase without a kinematic component (11-8 Ma); and 3) a compressional phase with thickening of the crust and lithosphere (8-0 Ma). We note, however, that our 1D modelling approach simplifies the problem to its first-order components and neglects the effects of lateral lithospheric heterogeneities (different tectonic units) and variations in the timing of main tectonic episodes in different parts of the Pannonian Basin system. These simplifications, as we will demonstrate through a sensitivity analysis, do not have a significant impact on the generalized interpretations presented. Extensive geological and geophysical studies of the sedimentary record (Balázs et al., 2016) and crustal and lithospheric structure (Horváth et al., 2006) as well as xenoliths brought to the surface by alkali basaltic melts (Embey-Isztin et al., 2014) have been used to constrain the depth level of the Moho and LAB in the pre-rift, syn-rift and present configuration (Falus et al., 2000; Kovács et al., 2012; Török, 2012).

a

b
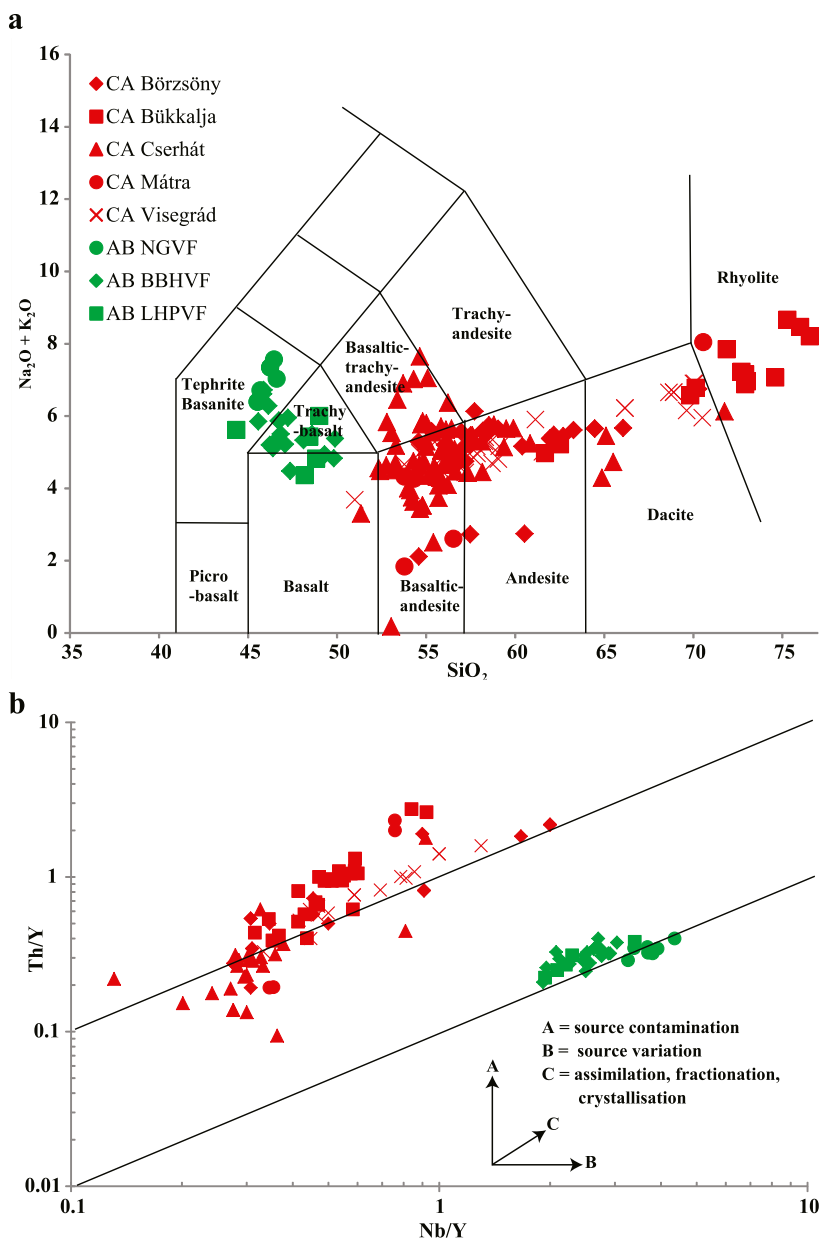
Fig. 2. a) Na$_2$O+K$_2$O vs. SiO$_2$ (Total Alkali Silicate: TAS) diagram for calc-alkaline rocks and alkali basalts from the Northwestern Pannonian Basin. The diagram is modified after Le Bas et al. (1986); b) Nb/Y vs. Th/Y diagram is modified after Seghedi et al. (2004). See text for further explanations. CA = calc-alkaline rocks; AB = alkali basalt, NGVF = Nógrád – Gömör Volcanic Field; BBHVF = Bakony-Balaton Highland Volcanic, LHPVF = Little Hungarian Plain Volcanic Field. Figures are modified after Fig. 2 and Fig. 4c in Kovács and Szabó (2008). See Suppl. Table 1 for sources of data for different locations.

Table 1
Parameters of kinematic model.

Phase of evolution	Time, t [Ma]	Crust		Lithosphere
		Moho, H_{crust} [km]	Upper/lower crust boundary, $H_{crust}^{upper}/H_{crust}$	Lithosphere-asthenosphere boundary (LAB), H_{lith} (T_L =1300 °C) [km]
Onset of extension	17	**60** (30-70)	**0.67** (0.33-1.0)	**130** (120-150)
End of extension	11	**20** (5-25)	**0.65** (0.35-1.0)	**55**
Onset of compression	8	**20** (5-25)	**0.65** (0.35-1.0)	Defined from model of thermal relaxation
Present-day	0	**25**	**0.6** (0.4-1.0)	Defined from model of thermal relaxation

Temporal variations of depth of crustal and lithospheric surfaces from onset of rifting to present-day corresponding to documented tectonic evolution in the Northwestern Pannonian Basin. Values in bold correspond to the reference model (Figs. 3–5), values in brackets provide a range of values adopted for the sensitivity analysis (Suppl. Figs. 4-7).

In the reference model, during the extensional phase (17-11 Ma) the Moho and LAB move upward at constant rates (∼6.5 km/Myr and 12.5 km/Myr, respectively) that thin the crust from 60 km to 20 km and reduce the total thermal lithosphere thickness (i.e. depth of the 1300 °C) from 130 km to 55 km (Table 1). Following the termination of the extensional phase (11-0 Ma), thickening of the mantle lithosphere is mostly a consequence of thermal relaxation. The crust remains at a constant thickness in the neutral

Table 2
Parameters of thermal model.

Surface temperature, T_0 [°C]	Temperature at LAB, T_{LAB} [°C]	Sublithosphere gradient [°C × km^{-1}]	Thermal capacity, c_p [J × kg^{-1} × K^{-1}]	Thermal conductivity, k [W × m^{-1} × K^{-1}]		Near surface heat production, A_0 [μW × m^{-3}]	Characteristic depth of heat source distribution, D [km]
				Crust	Mantle		
0	**1300**	**0.3**	**1000**	**2.5**	**3.5**	**6.0** (0.0-12.0)	**10** (2-16)

For the radiogenic heat production (A_r) we use the well-known assumption of its exponential decrease with depth: $A_r(z) = A_o \exp\left(-\frac{z}{D}\right)$. Values in bold correspond to the reference model (Figs. 3–5), values in brackets provide a range of values adopted for the sensitivity analysis (Fig. 6, Suppl. Fig. 3).

Table 3
Rheological and material properties.

Material	Density at normal conditions, ρ_0 [kg × m^{-3}]	Rheological parameters					
		Brittle/plastic		Ductile			
		Cohesion, C [MPa]	Internal friction angle, ϕ [°]	Pre-exponential constant, $\log(A_D)$ [Pa^n × s]	Activation energy, E [kJ × mol^{-1}]	Activation volume, V [cm^3 × mol^{-1}]	Power law exponent, n []
Upper crust	2700	5.0 ($\phi > 3.0$)	30.0 → 0.2	28.0	223	0	4.0
Lower crust	3000	or		21.05	445	0	4.2
Mantle	3300	0.5 ($\phi < 3.0$)		15.56	530	13	3.5

To relate the density (ρ) to temperature (T) and pressure (P) change, we use Boussinesq approximation: $\rho = \rho_0 [1 - \alpha(T - T_0)][1 + \beta(P - P_0)]$, where ρ_0 is density at normal conditions ($T_0 = 298$ K; $P_0 = 0.1$ MPa), $\alpha = 3\times10^{-5}$ K^{-1} is thermal expansion coefficient, and $\beta = 1\times10^{-5}$ MPa^{-1} is adiabatic compressibility. Data sources of rheological parameters are from Wilks and Carter, 1990; Gleason and Tullis, 1995; and Hirth and Kohlstedt, 2003.

phase (11-8 Ma) and is subject to a modest thickening from 20 to 25 km during subsequent compression due to tectonic shortening and magmatic underplating (8-0 Ma; e.g. Embey-Isztin et al., 1990). Over the entire simulation duration the crust is composed of a predominantly felsic composition where the upper crust makes up more than a half of the total crustal thickness (Table 1). This internal crustal structure adopted in the reference model is in accordance with geophysical observations showing that the present-day upper crust is ∼15 km whereas the lower crust is ∼10 km (Tari et al., 1999; Hetényi et al., 2015).

The kinematics of the reference model are consistent with quantitative estimates from subsidence history and evolution of lithosphere geometry (Lenkey et al., 2002; Horváth et al., 2006) and with present-day constraints on the crustal and lithospheric mantle structure from deep seismic reflection data (Posgay et al., 1995) and magneto-telluric studies (Ádám et al., 2017). However, given uncertainties and spatial variability in current and reconstructed estimates of the ratio between upper and lower crustal thickness and Moho depth, the sensitivity of our results to the model kinematics was tested through a systematic parameter study using the range of values specified in Table 1. The original position of the bottom of the thermal lithosphere was also varied within a depth range (Table 1) spanning estimates for the ambient present-day lithosphere thickness at the rim of the Pannonian Basin (Kovács et al., 2020).

Based on the kinematic model, the 1D thermal evolution was calculated. The initial temperature distribution within the lithosphere was approximated by the steady-state solution of the thermal production-diffusion equation for constant surface (0 °C) and LAB (1300 °C) temperatures. The parameters defining the exponential decay of radiogenic heat production with depth (near surface heat production and characteristic depth of heat source distribution) were varied over a very wide range (see values for reference and additional models in Table 2) to explore their impact on model predictions. The sublithosphere (mantle) geotherm at temperature >1300 °C was constrained by an adiabatic thermal gradient of 0.3 °C/km (Sleep, 2003). Subsequently, the thermal evolution is modelled in small timesteps where the temperatures are displaced according to the temporal displacements of the key lithospheric interfaces in the kinematic model and simultaneously recalculated by solving the heat diffusion equation (see Supplementary Methods). During the extensional phase we calculated temperatures for the lithosphere part of the model domain only, adopting constant

temperature boundary conditions: 0 °C and 1300 °C at the top and the bottom of the thermal lithosphere, respectively. In contrast, during the post-extensional neutral and compressional stages temperatures were calculated for the whole model with a constant temperature at the bottom boundary (200 km) after termination of extension. This implies that at the post-rift stage the bottom of the thermal lithosphere evolves through time, being subject to post-rift thermal relaxation, without a direct control on its position by the kinematic model.

Based on the temporal variations in calculated temperature distribution and in compositional stratification (i.e. changes in thicknesses of upper crustal and lower crustal layers), the rheological structure of the lithosphere at each time step was tracked for the entire life span of the model. The long-term strength of the lithosphere varies as a function of depth according to brittle and ductile deformation laws. Rheological parameters used in this study are provided in the Table 3. Similar to the rheological stratification of the lithosphere, the predicted thermal history allowed tracking the evolution of depth-distributed melting. See Supplementary Methods for more details.

4. Results

4.1. Reference model evolution and comparison with pertinent data for the Northwestern Pannonian Basin

Fig. 3 shows the results of the reference model for six key time slices from the initial steady-state thermal distribution of unextended crust and mantle lithosphere (Fig. 3a) through their maximum stretching and thinning (Fig. 3c) to the present-day configuration (Fig. 3f). The overall bulk strength of the lithosphere is characterized by a reduction during the extension stage (17-11 Ma; Fig. 3a-c) and an increase due to post-rift healing due to thermal cooling combined with modest thickening of the crust (8-0 Ma; Fig. 3d-f). At the same time, and most importantly, the internal thermo-rheological structure of the lithosphere is subject to pronounced temporal variations during model evolution (Fig. 3).

The final state (present day) of the rheological profile calculated for an internal friction angle (ϕ) of 20° (blue dashed line) is characterized by a rheologically stratified brittle-ductile crust underlain by almost entirely ductile mantle (Fig. 3f). Such an estimate of the thermo-rheological structure in the present-day Pannonian Basin is in agreement with previous thermal and rheological models of the
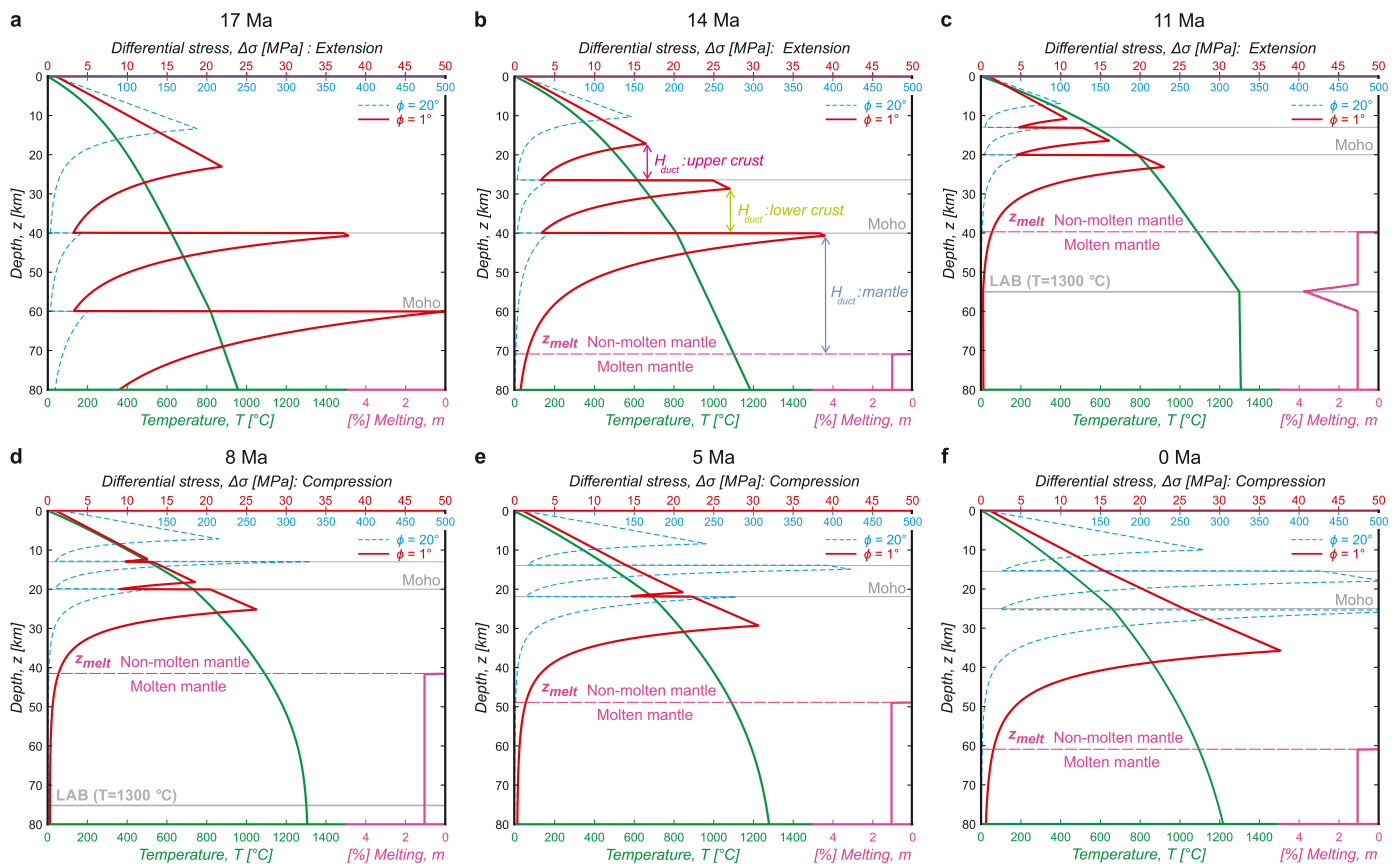
Fig. 3. Results of the reference thermo-kinematic model for the evolution of the temperature (green line), rheological strength (dashed blue and solid red line for internal friction angle (ϕ) of 20° and 1°, respectively), and melting degree (magenta line). The boundary between upper and lower crust, Moho, and bottom of the thermal lithosphere (lithosphere-asthenosphere boundary – LAB, an isotherm of 1300 °C) are shown by gray lines. The boundary between molten and non-molten mantle (z_{melt}) is indicated by magenta line. Upper panels (a-c) correspond to syn-rift phase of gradual tectonic stretching and associated thinning of the crust and mantle lithosphere. Bottom panels (d-f) illustrate post-rift phase of thermal relaxation accompanied by tectonic compression. Depending on mode of dominating tectonic deformation, differential brittle stress is calculated according to formulation for extensional (a-c) or compressional (d-f) state (see Supplementary Methods). Note overall decoupled rheological structure when $\phi = 20°$ (dashed blue line) and temporal transition from decoupled lithosphere during extensional phase to the complete mechanical coupling during the final phase of post-rift evolution for melt-weakened friction angle ($\phi = 1°$; solid red line). The integrated thicknesses of the ductile layers defined for rheological profile with $\phi = 1°$ in the upper/lower crust and lithospheric mantle are marked by H_{duct} in the panel "b" (see also their temporal evolution in Fig. 4c). Note different horizontal scales for the ambient (blue line) and melt-weakened (red line) deviatoric stress profiles.

European lithosphere (Tesauro et al., 2009) and the distribution of earthquake focal depths occurring to a maximum depth of 20 km (bottom of brittle lower crust) with a maximum concentration of events at 6-10 km depth (brittle upper crust), and complete lack in the mantle (Tóth et al., 2002).

We explored the consequences of variations in the parameters for plastic (frictional or brittle) deformation (cohesion and internal angle of friction; see Table 3) that are known to be subject to major reduction due to strain- and/or fluid-related softening/weakening (Huismans and Beaumont, 2003; Gerya et al., 2015). In particular, when the strength in the brittle regime is calculated using a characteristic melt-softened internal friction angle ($\phi = 1°$; red solid line in Fig. 3), the thermo-rheological structure of the melt-weakened lithosphere evolves from a decoupled profile during the entire extensional phase to whole lithospheric mechanical coupling (i.e. to disappearance of the ductile layers within the crust) at the final stage of post-rift thermal relaxation.

In the model we assume that the transition between partially molten and non-molten upper mantle (z_{melt}) roughly corresponds to an isotherm of 1100 °C following the (pargasite) dehydration solidus (Suppl. Fig. 1). It emerges that in high heat flow areas (i.e. such as a highly extended continental lithosphere) it is intrinsically ∼20-40 km shallower (see Fig. 4a) than the bottom of the thermal lithosphere (LAB) which is defined by an isotherm of 1300 °C for the volatile-free and non-molten mantle. Striking

temporal variations occur at the depth of z_{melt}: the depth of the molten upper mantle rises linearly from 100 km to 40 km during the extension phase (Fig. 3a-c) followed by gradual sinking until 60 km at present-day (Fig. 3d-f). Given that even incipient partial melting of the upper mantle leads to an immediate drop in its effective viscosity (Kohlstedt, 1992), it is more relevant to consider the transition to the molten mantle as a boundary between lithosphere and asthenosphere. This observation contributes to reconciling current controversies about the definition of the LAB (Eaton et al., 2009). The model predictions for z_{melt} can be therefore directly compared with published data on the evolution of lithospheric thickness. Seismic anisotropy data and upper mantle xenoliths (Kovács et al., 2012) suggest asthenosphere uplift to 40 km at the end of the syn-rift phase (11 Ma) and subsequent deepening to a level of 60 km in the centre of the Northwestern Pannonian Basin at present-day (0 Ma). These observations are in close agreement with model estimates for z_{melt} (Fig. 4a).

Another observable for direct comparison with model predictions is the surface heat flow (q_0). The modelled surface heat flow shows a peak (∼140 mW/m^2) at the termination of extension followed by a decay to ∼90 mW/m^2 (Fig. 4b) that is slightly lower than average estimates for present-day heat flow in the region (Lenkey et al., 2002).

The cumulative amount of melt (M) is calculated as an integrated value of melting degree (m) over the depth between the
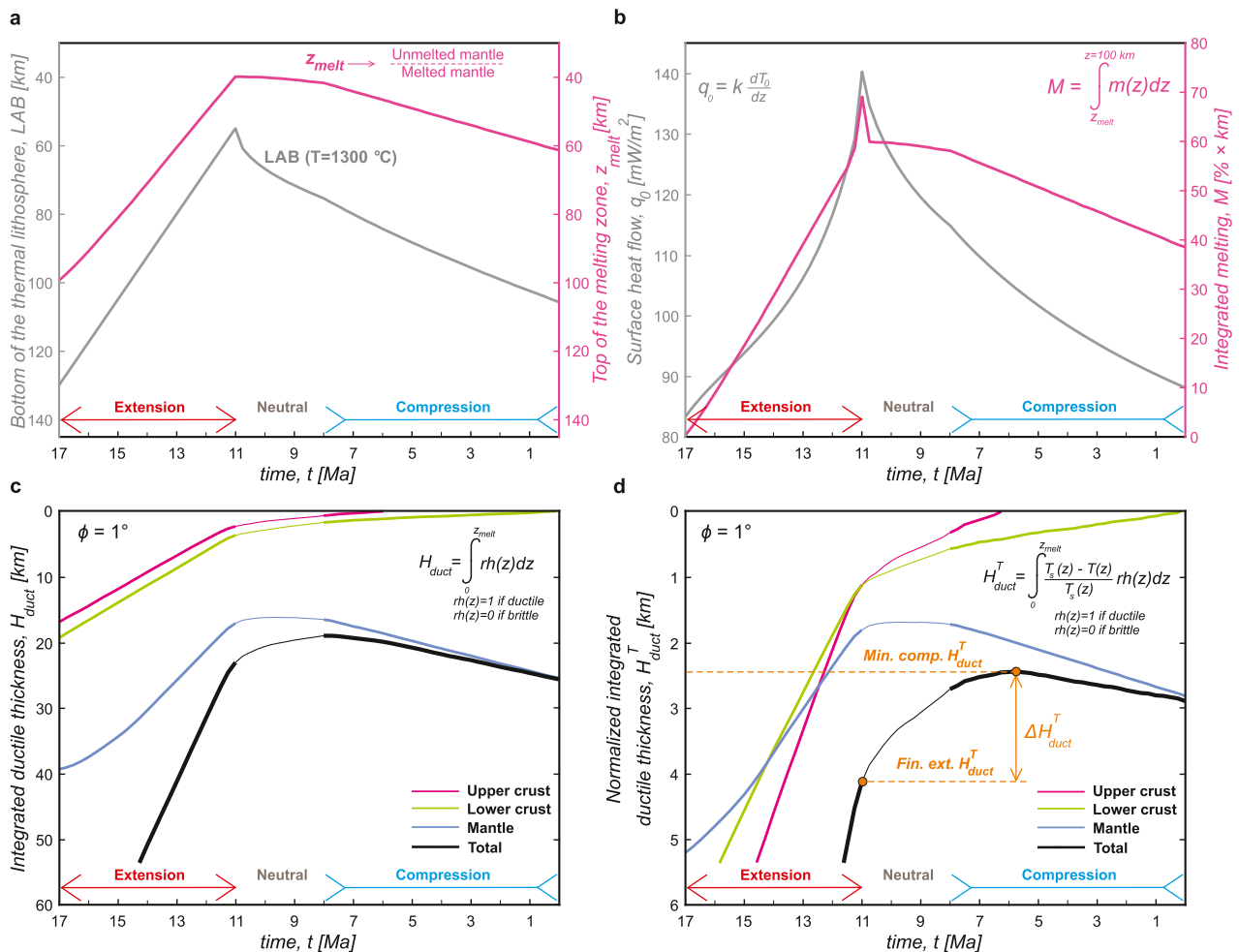
Fig. 4. Temporal evolution of the predictions from the reference thermo-kinematic model. a) bottom of the thermal lithosphere (lithosphere-asthenosphere boundary – LAB, an isotherm of 1300 °C; gray line) and transition between partially molten mantle and overlying mantle not affected by melting (z_{melt}; magenta line); b) surface heat flow (q_0; gray line) and cumulative amount of melt (M; magenta line); c) integrated thickness of ductile layers (H_{duct}) within upper (magenta line) and lower (green line) crust, mantle (blue line) and whole lithosphere (black line). Thin line segment corresponds to tectonically neutral stage of the system development; d) normalized integrated thickness of ductile layers (H_{duct}^T). Figure conventions as in panel "c". H_{duct} and H_{duct}^T are calculated from rheological profiles defined for melt-weakened friction angle ($\phi = 1°$). The total H_{duct}^T (black line in panel "d") represents a quantitative measure for the probability of alkali basaltic magmatism over geological history (lower total H_{duct}^T –> higher probability). ΔH_{duct}^T stands for the difference between H_{duct}^T at the end of extensional phase ("Fin. ext. H_{duct}^T") and minimum value of H_{duct}^T during compressional phase ("Min. comp. H_{duct}^T").

top of the molten zone (z_{melt}) and 100 km (z_{melt} at the model's onset). It gradually increases during the extensional phase with a short-lived spike at the end of the extension related to overstepping of the dry solidus temperature (Fig. 3c) and slowly decays during the post-extensional period (Fig. 4b).

As mentioned above, for the emplacement of volcanics at the surface two conditions must be fulfilled: 1) presence of melts in the asthenosphere, which appears to be the case during the entire life span of the Miocene-Present evolution of the Northwestern Pannonian Basin (see evolution of z_{melt} and cumulative amount of melt (M) in Fig. 4a and 4b, respectively); and 2) presence of conduits inside the overlying lithosphere. Faults formed in the brittle part of the lithosphere provide effective conduits for fast upward migration of melts from their source region or magma plumbing system (Kovács et al., 2020). In contrast, it is well known that ductile layers are not providing optimal mechanical conditions for formation of conduits for emplacement of melts through the lithosphere to the surface (Gerya and Burg, 2007; Colón et al., 2018), with relatively slow quasi-vertical infiltration and potential loss of melts and contamination with crustal material. Experimental and theoretical evidence exists that, if the amount of partial silicate melt remains low ($\sim <2$ v/v%), melts can be effectively retained

in the upper mantle in the absence of tectonic forcing (Faul, 2001). The maximum degree of partial melting in the asthenosphere under the Pannonian Basin system is within this range (e.g. Seghedi et al., 2004; Harangi et al., 2015). Fig. 4c represents the temporal evolution of the integrated ductile thicknesses (H_{duct}; see Supplementary Methods) estimated for (1) upper and (2) lower crust, (3) the lowermost lithosphere (defined by the distance between the level of intra-mantle brittle-ductile transition and z_{melt}; see Fig. 3b) and (4) their sum.

During the syn-rift stage the gradual decrease in the thicknesses of the crustal layers and mantle lithosphere imposed by the kinematic model (Table 1) naturally leads to thinning of the ductile layers in the strength profile as well (Fig. 4c). However, simultaneous heating of the lithosphere due to a shallowing of the asthenosphere dome acts in an opposite direction, maintaining the existence of ductile low-viscosity intra-lithospheric layers until the cessation of the extensional phase. In case of a rheological profile defined for a characteristic melt-weakened friction angle ($\phi = 1°$), the crustal ductile layers that are already relatively thin (<5 km) at the end of extension (11 Ma), completely disappear during subsequent cooling of the lithosphere leading to the establishment of a complete rheological coupling inside the lithosphere at ~ 0.5-1

Ma (Figs. 3 and 4c). The total H_{duct} (black line in Fig. 4c) reaches the minimum with the termination of the neutral phase (8 Ma) after which it is characterized by a gradual increase during the entire compressional phase (8-0 Ma). This growth of the aggregate thickness of the ductile layers is conditioned by a significant thickening of the mantle ductile layer during thermal relaxation (blue line in Fig. 4c) that overcomes simultaneous thinning and disappearance of the crustal ductile channels (magenta and green lines in Fig. 4c). The thickening of ductile mantle is, in turn, related to deepening of z_{melt} that appears to be faster than the simultaneous increase in the depth of the brittle-ductile transition in the mantle lithosphere.

A complementary and probably even more robust criterion for assessment of effectiveness of melt transfer through the lithosphere includes not only thicknesses of the ductile layers (H_{duct}) but also the contrast between ambient temperatures $T(z)$ at the corresponding depths and the temperature of the solidus $T_s(z)$ at these levels. The estimate for integrated ductile thickness normalized by the coefficient $\frac{T_s(z)-T(z)}{T_s(z)}$ (see Supplementary Methods) is referred below as H_{duct}^T (Fig. 4d). The minimum in total H_{duct}^T occurs under a compressional tectonic regime at $\sim$5.75 Ma, just after the disappearance of the upper crustal ductile layer ($\sim$6.5 Ma). Given the stronger contrast between ambient temperatures $T(z)$ and solidus $T_s(z)$ at shallow depths, the contribution of a crustal ductile channels to the total value of H_{duct}^T is more significant than in the case of non-normalized ductile thicknesses (H_{duct}). Therefore, the post-rift thinning of the crustal ductile layers results in a pronounced decrease in total H_{duct}^T during the time interval of 11-5.75 Ma despite the simultaneous thickening of the mantle ductile zone and corresponding increase of mantle H_{duct}^T. Subsequently (5.75-0 Ma), the total H_{duct}^T gradually increases similarly to the total non-normalized H_{duct}.

Combining the temporal distribution of the cumulative melting M (Fig. 4b) with findings on time evolution of H_{duct}^T (Fig. 4d) provides a self-consistent explanation for the observed temporal variations of both volumes and composition of the volcanism in the Northwestern Pannonian Basin (Fig. 1b). The maximum value of melting degree (m; Fig. 3c) and the peak of cumulative amount of melting (M; Fig. 4b) occur at the termination of extension (11 Ma), when the lithosphere is stretched and thinned the most but is still rheologically decoupled: under the condition of a melt-weakened friction angle ($\phi = 1°$), H_{duct}^T of the upper and lower crust are both >1 km (Fig. 4d). These predictions roughly coincide with the observed maximum in calc-alkaline (contaminated) volcanic activity (even if the observations are ambiguous – see e.g. Pécskay et al., 2006; Szakács et al., 2018). Therefore, initially primitive and uncontaminated basaltic melts went through significant fractionation and assimilation in the crust leading to the formation of voluminous calc-alkaline intermediate and felsic magmas (Seghedi et al., 2004; Kovács and Szabó, 2008). Although basaltic magmas did not come to the surface this time, there is evidence for large scale basaltic underplating at the Moho and fractionation in the upper mantle (e.g. Embey-Isztin et al., 1990). The small deviation between predicted and observed times for maximum calc-alkaline magmatic activity arises from the limitations of the model that assumes a constant rate of syn-rift thinning and coeval tectonic deformation over the entire basin and does not include horizontal variations in crustal and lithosphere structure. Another component of this discrepancy could also reside in the large ambiguity in estimates for both volumes (Karátson and Timár, 2005) and ages (e.g. Pécskay et al., 2006; Szakács et al., 2018) of the syn-rift calc-alkaline magmatism. The accurate quantitative assessment of these volumes obviously requires further studies measuring the surface and sub-surface volumes of magmatic bodies.

As mentioned above, the total H_{duct}^T is a quantitative proxy for assessment of the capacity of the lithosphere to transport asthenospheric melts to the surface: lower values of the total H_{duct}^T correspond to higher effectiveness of melt transmission and, therefore, higher probability for shallow emplacement of deep-sourced magmas. In our model, the total H_{duct}^T reaches a minimum at 5.75 Ma (Fig. 4d) that only slightly precedes the onset of intensive alkali basaltic (uncontaminated) volcanism (5 Ma) as reported in the Northwestern Pannonian Basin (Fig. 1b). The cumulative amount of basaltic magma in the upper mantle (M) is lower at this moment than at the peak of calc-alkaline volcanism. This is consistent with less voluminous magmatism during the post-rift phase (Kereszturi et al., 2010) even if the model cannot provide a quantitative estimate of the intensity of volcanism especially in the context of a comparison between calc-alkaline and alkali stages. Given that the minimum of the total H_{duct}^T occurs when the lithosphere is almost completely mechanically coupled (H_{duct}^T of the upper and lower crust are 0 and $\sim$0.5 km, respectively), a deficiency of intermediate crustal chambers might be expected. Therefore, a style of volcanism without crustal contamination and fractionation is plausible.

The effects of the variation in characteristic melt-weakened internal angles of friction (ϕ) on the resulting rheological structure are summarized in Fig. 5. For all values of ϕ that are higher than 1°, the lithosphere remains rheologically decoupled over the entire time span of the system evolution. In contrast, for the lowest values of internal frictional angle ($\phi \le 0.2°$), the lithosphere becomes mechanically coupled even before the termination of extension (11 Ma). A temporal transition from decoupling at termination of rifting (11 Ma) to coupling during the post-rift compressional phase (8-0 Ma) occurs only for a relatively narrow range of ϕ (0.4-1.0°; green asterisks on the graph of Fig. 5b2). These values agree well with previous estimates of characteristic melt-weakened large-scale lithospheric friction coefficients in both oceanic (Gerya et al., 2015) and continental (Bahadori and Holt, 2019) environments and suggest that there should be some rheological feedback mechanism that stabilizes melt-induced lithospheric strength reduction within this relatively narrow range.

Here we introduce a new parameter ΔH_{duct}^T that refers to the difference between H_{duct}^T at the end of extensional phase and the minimum value of H_{duct}^T during the compressional stage (see also Fig. 4d). ΔH_{duct}^T provides a fair quantitative proxy on the expected relative intensity of basaltic magmatism before and after termination of extension: negative values of ΔH_{duct}^T attest a higher probability of syn-rift alkali basaltic volcanism whereas positive ones are in favour of more intense deep-sourced volcanic activity after the end of rifting. The highest positive ΔH_{duct}^T is thus the most consistent with observed late stage alkali basaltic volcanism after the cessation of rifting (in Fig. 5b2 it corresponds to $\phi = 1°$). A compressional mode of brittle deformation requires higher differential stresses than extension (this difference could reach up to $\sim$3 times when $\phi = 30°$, see Supplementary Methods). Therefore, a switch to compressional tectonics between 11 and 8 Ma leads to an abrupt thickening of all ductile layers and, therefore, to a stepwise increase in their sum (total H_{duct}), that is undistinguishable for the lowest ϕ (0.2-1.0°) but becomes more and more pronounced with further increases in ϕ (see Fig. 5b1). Combined with faster thickening of the mantle ductile zone for higher ϕ, this leads to negative values of ΔH_{duct}^T for all $\phi \ge 10°$ (Fig. 5b2). In contrast, ΔH_{duct}^T is always positive if $\phi \le 8°$. That means that our conclusions on the rheological control on the magmatic evolution remain valid not only for an extremely reduced ϕ (0.4-1.0°) but also under condition of much more moderate softening of a frictional-plastic rheology with ϕ up to 8°.

Given that the earliest stage of system evolution is characterized by a low amount of melting in the mantle (Fig. 4b), it is unlikely to expect a significant melt-induced weakening at this time.
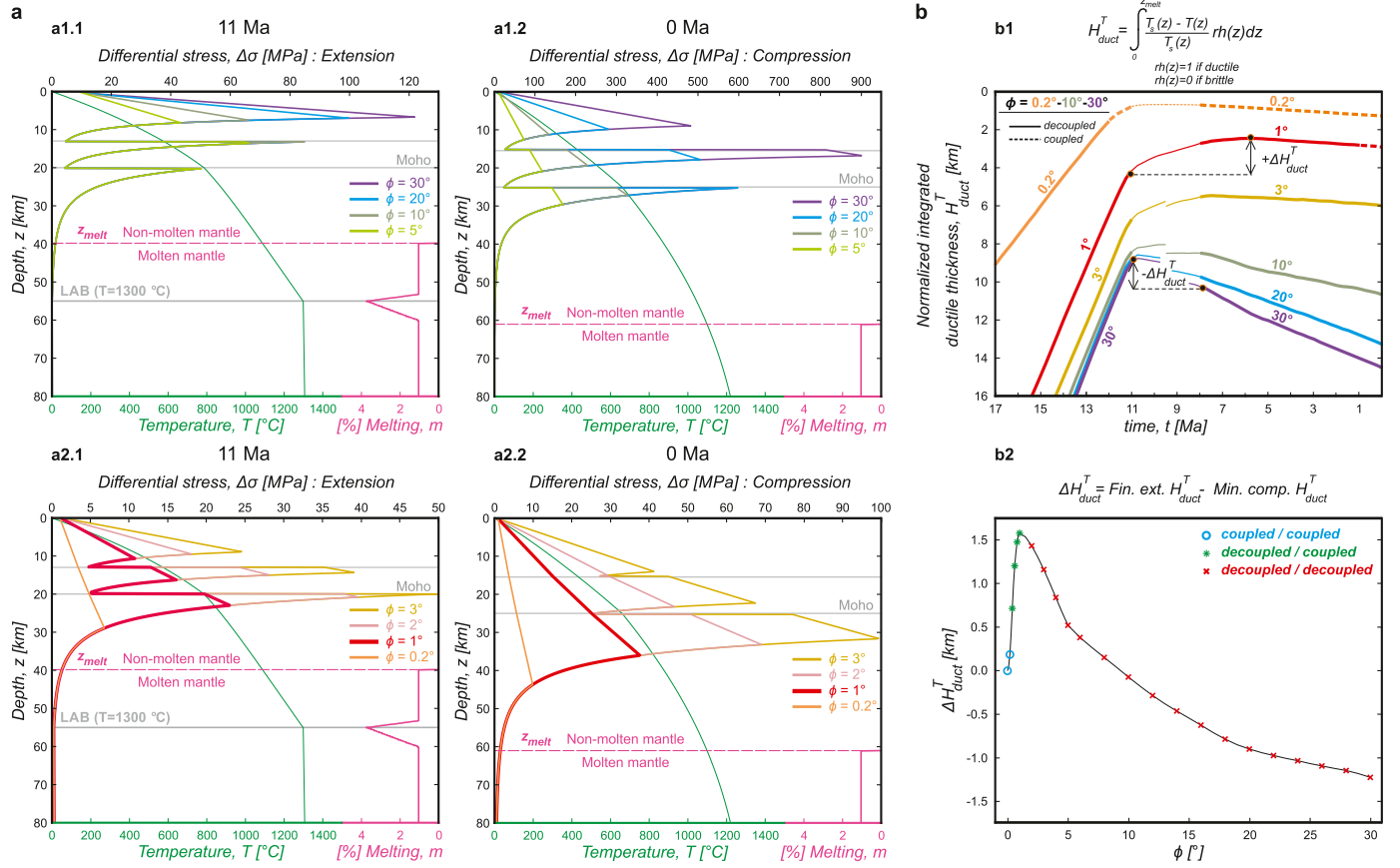
Fig. 5. The reference thermo-kinematic model and the variable internal angles of friction (ϕ). a) Rheological structures on two key time slices (maximum stretching and thinning at 11 Ma and present-day post-relaxation state at 0 Ma) are shown for internal friction angles (ϕ) ranging from 30° to 5° (a1) and from 3° to 0.2° (a2); b1) temporal evolution of total normalized integrated ductile thickness (total H_{duct}^T) for ϕ of 0.2-1-3-10-20-30° shown by lines of colours as in panel "a". Dashed and solid segments of the lines refer to coupled and decoupled lithosphere, respectively. Note positive ΔH_{duct}^T for $\phi = 1°$ (see also Fig. 4d) and negative ΔH_{duct}^T for $\phi = 30°$ attesting to higher probability of uncontaminated alkali volcanism at the post- and syn-rift stages, respectively; b2) ΔH_{duct}^T as a function of internal friction angle (ϕ). Blue circles show the models where the lithosphere is mechanically coupled both at the end of extensional stage and at the present-day; green stars mark the experiments with decoupled lithosphere at the end of extension switched to the coupled mode at the present-day; red crosses label the models with decoupled rheology both at the termination of extensional phase and at the present-day. Note that ΔH_{duct}^T remains positive when ϕ is lower than ~8°.

Therefore, in addition to the models with constant values of ϕ (Suppl. Fig. 2a, d), a continuous decrease of the internal friction angle (ϕ) through time was explored (Suppl. Fig. 2b, c). The gradual transition from an ambient friction angle of 20° at 17 Ma through an intermediate value of ~13° at the termination of rifting (11 Ma) to a melt-weakened angle of 1° at 0 Ma was adopted in the experiment shown in Suppl. Fig. 2b. This model gives a positive value of ΔH_{duct}^T which is higher than in the experiment assuming a characteristic melt-weakened friction angle ($\phi = 1°$) over the entire model evolution (Suppl. Fig. 2d). However, in this case the total H_{duct}^T reaches a minimum at 0 Ma (Suppl. Fig. 2b) that is 5-3 Myr later than the reported maximum of alkali basaltic volcanism in the Northwestern Pannonian Basin (Fig. 1b). In another additional simulation (Suppl. Fig. 2c), ϕ evolves in conjunction with the expected amount of melt (Fig. 4b) and decreases from high values during the melt-absent/melt-poor stages ($\phi = 20°$ at 17 Ma) to melt-weakened values ($\phi = 1°$) at the end of extension (11 Ma) when the cumulative amount of melt (M) reaches its maximum value. In this case, the post-rift evolution of the normalized integrated ductile thicknesses (H_{duct}^T) expectedly repeats that of the model with a constant melt-weakened friction angle ($\phi = 1°$) resulting in the same value of ΔH_{duct}^T (compare Suppl. Fig. 2c and 2d). Therefore, in order to maintain simplicity of the analysis of model parameters, we assume the internal friction angle to be constant in time for all other experiments.

4.2. Sensitivity analysis

To explore the sensitivity of the model to differences in inputs (see Tables 1–2), we varied six controlling parameters: 1) near surface heat production (A_0); 2) characteristic depth of heat source distribution (D); 3) initial thickness of the crust (H_{crust}^{init}; i.e. H_{crust} at 17 Ma); 4) thickness of the crust at the termination of thinning (H_{crust}^{thin}; i.e. H_{crust} at 11 Ma); 5) portion of the upper crust in the total crust thickness ($H_{crust}^{upper}/H_{crust}$), and 6) initial thickness of the thermal lithosphere (H_{lith}^{init}; i.e. depth level of LAB at $t = 17$ Ma).

In case of a rheological profile calculated for melt-weakened friction angles ($\phi = 1°$ and $\phi = 3°$), near surface heat production (A_0; Fig. 6) provides a wide range of values resulting in positive ΔH_{duct}^T (0.0-12.0 µW/m³ and 0.0-10.0 µW/m³, respectively). Moreover, ΔH_{duct}^T remains close to 0 when A_0 is 0.0-6.0 µW/m³ for $\phi = 10°$, whereas it is continuously negative for $\phi = 20°$ over the entire range of tested A_0. The highest positive ΔH_{duct}^T under $\phi = 1°$ corresponds to values A_0 of 8.0-10.0 µW/m³ (Fig. 6b). However, such high values of A_0 fall out of the range corresponding to the temporal transition between decoupled and coupled mode of the lithosphere rheological stratification (0.0-6.0 µW/m³) and correspond to lowered ΔH_{duct}^T for $\phi = 3°$ and $\phi = 10°$. Moreover, they lead to overestimation of present-day heat flow (Fig. 6d) and exceed usual rock estimates of A_0 (Artemieva and Mooney, 2001). The depth level of the transition between molten and non-molten
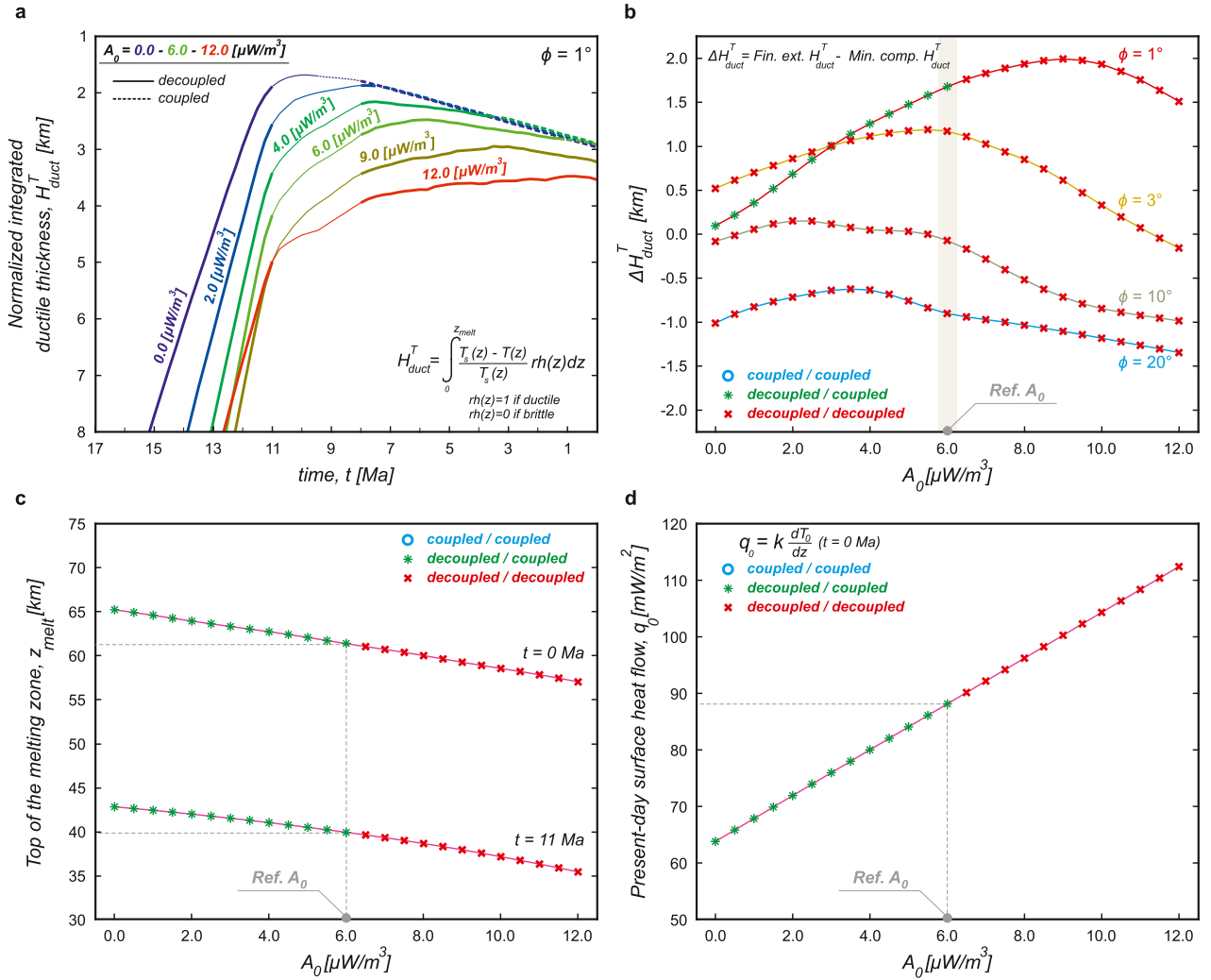
Fig. 6. Results of parametric analysis for different values of heat production in near-surface rocks (A_0). a) temporal evolution of total normalized integrated ductile thickness (total H_{duct}^T calculated from rheological profiles with melt-weakened friction angle: $\phi = 1°$) for A_0 of 0.0-2.0-4.0-6.0-9.0-12.0 μW/m³ shown by lines of colours gradually changing from blue (minimum value of $A_0 = 0.0$ μW/m³) through green (reference value of $A_0 = 6.0$ μW/m³) to red (maximum value of $A_0 = 12.0$ μW/m³); b) ΔH_{duct}^T calculated for ϕ of 1-3-10-20° as a function of A_0; c) top of partially molten mantle at the end of the syn-rift phase (11 Ma) and present-day (0 Ma) as a function of A_0; d) present-day surface heat flow (q_0 at $t = 0$ Ma) as a function of A_0.

mantle (z_{melt}) at 11 and 0 Ma (Fig. 6c) varied in the range ± 5 km with respect to "best-fit" values ($\sim$40 km and $\sim$60 km, respectively) that are reproduced in the reference model ("Ref. A_0" of 6.0 μW/m³).

The analysis of the second parameter controlling crustal heat generation (D) also points out a broad range of values compatible with the scenario of late stage alkali basaltic volcanism after the cessation of rifting (positive ΔH_{duct}^T) with preferential value of reference $D = 10$ km (Suppl. Fig. 3).

The reference value of initial thickness of the crust ($H_{crust}^{init} = 60$ km) has been adopted in view of the paleo-reconstructions (Kovács et al., 2012) assuming considerable pre-rift thickening related to preceding Alpine orogenic processes (Török, 2012). However, lower H_{crust}^{init} of 45-55 km not only result in positive ΔH_{duct}^T when ϕ is 1-3° but also correspond to its maximum values for higher ϕ (10°-20°). That means that moderate pre-rift crustal thicknesses (e.g. H_{crust}^{init} of 45 km) are also consistent with observed scenarios of magmatic evolution (Suppl. Fig. 4).

Depending on adopted ϕ, maximum ΔH_{duct}^T could be reached under conditions of moderate, middle or major crustal thinning during the syn-rift phase ($H_{crust}^{thin} = $ 20-25, 12-16 and 8-12 km, respectively; Suppl. Fig. 5b). The value H_{crust}^{thin} of 20-25 km (that

is close to present-day crustal thickness) seems to be preferential in view of 1) previous geological reconstructions assuming moderate to zero crustal thickening during post-rift inversion (Kovács et al., 2012) and 2) experimental evaluations of the present-day heat flow that is considerably underestimated in the models with decreased H_{crust}^{thin} (Suppl. Fig. 5d).

Additional experiments exploring the internal structure of the crust (Suppl. Fig. 6) show that a predominantly felsic composition of the crust ($H_{crust}^{upper}/H_{crust} > 0.5$) is crucial to reproduce rheological decoupling at the level of the upper crust during syn-rift extension. However, a strong mafic layer in the lowermost crust is essential to avoid the decoupling from the mantle lasting until present-day. Higher ratios of felsic upper crust composed of radiogenic-enriched rocks ($\sim$0.65 of the total crustal thickness as adopted in reference model) are in agreement with our independent analysis on heat production parameters (A_0 and D; see Fig. 6 and Suppl. Fig. 3), which "best-fit" values are closer to the upper limits of their usual measured estimates (Artemieva and Mooney, 2001). In contrast to the internal structure of the crust, the initial depth of the 1300 °C isotherm (H_{lith}^{init}) has a much more modest influence on the general style of thermo-rheological profiles at the different stages of model evolution (Suppl. Fig. 7).
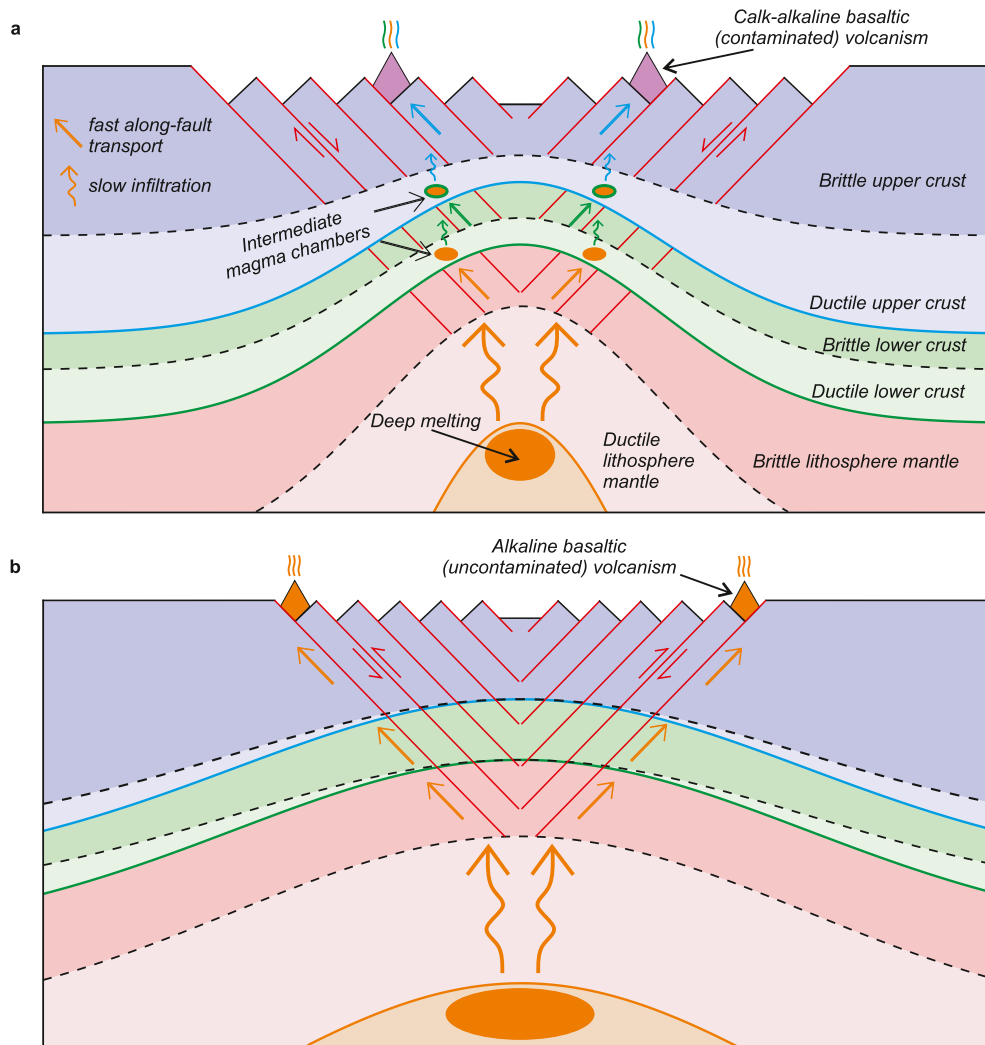
Fig. 7. Two principal modes of thermo-rheological stratification of the lithosphere and associated fault patterns controlling geochemical composition and spatial location of intracontinental volcanism. a) syn-rift phase: upper/lower crust ductile layers favour formation of intermediate magmatic chambers and crustal fractionation/assimilation of initially primitive basaltic melts leading to voluminous calc-alkaline (contaminated) volcanism preferentially concentrated in the basin interiors. Note that melts arising from these intermediate magma chambers in the ductile crust upon reaching overlying brittle layers could not immediately encounter overlying faults. This implies that melts have to percolate even much slower in the bottom part of the brittle layer than in the underlying ductile zones (prior to reaching the fault). As a consequence, the real value of H_{duct}^T (shown in Fig. 4d) may be underestimated when the lithosphere is strongly decoupled as it does not take into account this less favourable pathway for melts through the brittle segments of the crust distant to faults; b) post-rift thermal relaxation and tectonic inversion: the melted material of the asthenosphere percolates through the lowermost ductile segment of the lithosphere to be quasi-instantaneously transported to surface along deep-seated lithospheric-scale faults crossing uninterruptedly through the brittle part of rheologically coupled lithosphere. In contrast to the case shown in panel "a", resulting volcanism is concentrated at the basin margins and characterized by alkali basaltic (uncontaminated) composition. Quick transport of melts alongside brittle fractures is indicated by straight arrows trending parallel to fault planes whereas slow infiltration of the melt material in roughly vertical direction through ductile layers is shown by curved arrows.

5. Discussion and conclusions

To explain volumetric and compositional changes in the distribution of volcanism in continental back-arc tectonic settings several critical factors should be taken into account. The first one is the amount of melting residing in the asthenosphere. The second one is the capability of the overlying lithosphere to provide the conduits for melt emplacements to the surface. From this point of view, the variations in thickness of ductile layers in the crust appear to be of paramount importance. Our model suggests that after the beginning of the lithospheric extension and mantle melting the thermo-rheological structure of the melt-weakened lithosphere paradoxically evolves from a decoupled profile during the entire extensional phase to whole lithospheric mechanical coupling at the final stage of post-rift thermal relaxation.

Fig. 7 schematically illustrates how different modes of mechanical coupling/decoupling and associated fault patterns control the geochemical composition and spatial location of intracontinental volcanism. In the case of a rheologically coupled overlying lithosphere (i.e. lithosphere deprived of ductile layers in the crust or containing ductile crustal channels of reduced thickness), the melted material of the asthenosphere has to first percolate through the ductile segment of the lithosphere (curved arrows in Fig. 7b). Subsequently, melts encounter deep-seated faults cross-cutting the remaining part of the lithosphere to be quasi-instantaneously transported to the surface without any crustal contamination along its pathway (straight arrows in Fig. 7b). In contrast, melts penetrating through a rheologically decoupled overlying lithosphere are confronted with thick ductile layers in the lower and upper crust that favour the formation of intermediate magmatic chambers and possible fractionation and contamination with crustal material (Fig. 7a). As a consequence of the intrinsic faulting geometry, calc-alkaline volcanoes tend to be more concentrated to the interior of the area affected by lithospheric extension (Fig. 7a). In

contrast, alkali volcanism during the inversion phase appears to be more developed at the margins (Fig. 7b). Unfortunately, the current level of knowledge on the accurate spatial distributions of magmas does not permit to test this model prediction.

Although our 1D modelling approach disregards lateral variations in the crustal and lithosphere structure and non-simultaneity in geological time of the main tectonic episodes within different parts of the study area, our models provide testable predictions for a range of independent geological, geophysical and geochemical observables: 1) geochemical composition, temporal variations in intensity and spatial distribution of the volcanism; 2) reconstructed thicknesses of the lithosphere defined in terms of the transition between non-molten and molten mantle; and 3) measured present-day surface heat flow. Moreover, the parametric analysis evaluated a wide range of independent inputs for both thermal and kinematic parts of the model and provides additional and independent constraints for 1) radiogenic heat generation in the crust and 2) the crustal and lithosphere structures in the past and present. In view of the intrinsic non-uniqueness in interpretations of the model results due to uncertainties in model inputs, the purpose of our sensitivity analysis is not to identify the single solution that satisfies all observations. Instead, we aim to map the range of thermal parameters and kinematic scenarios which are consistent with the tectono-magmatic records in the studied area.

Although our study is based on parameters from the Northwestern ALCAPA unit of the Pannonian Basin system as a natural laboratory, our findings are broadly applicable in their scope in light of commonly observed transitions of calc-alkaline to basaltic volcanism elsewhere. The reason for these transitions is still disputed and attributed to a number of mechanisms. Our modelling, by taking into account the consequences of the temporal evolution of lithospheric rheology, provides a novel explanation for shifts in geochemistry of magmatism frequently observed in intracontinental rifting and back-arc settings.

Declaration of competing interest

The authors declare that they have no known competing financial interests or personal relationships that could have appeared to influence the work reported in this paper.

CRediT authorship contribution statement

All persons who meet authorship criteria are listed as authors, and all authors certify that they have participated sufficiently in the work to take public responsibility for the content, including participation in the concept, design, analysis, writing, or revision of the manuscript. Furthermore, each author certifies that this material or similar material has not been and will not be submitted to or published in any other publication before its appearance in the Earth and Planetary Science Letters.

Acknowledgements

Appendix A. Supplementary material

Supplementary material related to this article can be found online at https://doi.org/10.1016/j.epsl.2021.116925.

References

Ádám, A., Szarka, L., Novák, A., Wesztergom, V., 2017. Key results on deep electrical conductivity anomalies in the Pannonian Basin (PB), and their geodynamic aspects. Acta Geod. Geophys. 52 (2), 205–228.

Artemieva, I.M., Mooney, W.D., 2001. Thermal thickness and evolution of Precambrian lithosphere: a global study. J. Geophys. Res., Solid Earth 106 (B8), 16387–16414.

Bahadori, A., Holt, W.E., 2019. Geodynamic evolution of southwestern North America since the Late Eocene. Nat. Commun. 10, 5213.

Balázs, A., Matenco, L., Magyar, I., Horváth, F., Cloetingh, S.A.P.L., 2016. The link between tectonics and sedimentation in back-arc basins: new genetic constraints from the analysis of the Pannonian Basin. Tectonics 35 (6), 1526–1559.

Colón, D.P., Bindeman, I.N., Gerya, T., 2018. Thermomechanical modeling of the formation of a multilevel, crustal-scale magmatic system by the Yellowstone plume. Geophys. Res. Lett. 45, 3873–3879.

Coulon, C., Megartsi, M.H., Fourcade, S., Maury, R.C., Bellon, H., Louni-Hacini, A., Cotten, J., Coutelle, A., Hermitte, D., 2002. Post-collisional transition from calc-alkaline to alkaline volcanism during the Neogene in Oranie (Algeria): magmatic expression of a slab breakoff. Lithos 62 (3–4), 87–110.

Duggen, S., Hoernle, K., van den Bogaard, P., Garbe-Schönberg, D., 2005. Post-collisional transition from subduction-to intraplate-type magmatism in the westernmost Mediterranean: evidence for continental-edge delamination of subcontinental lithosphere. J. Petrol. 46 (6), 1155–1201.

Eaton, D.W., Darbyshire, F., Evans, R.L., Grütter, H., Jones, A.G., Yuan, X., 2009. The elusive lithosphere-asthenosphere boundary (LAB) beneath cratons. Lithos 109 (1–2), 1–22.

El Bakkali, S., Gourgaud, A., Bourdier, J.L., Bellon, H., Gundogdu, N., 1998. Post-collision neogene volcanism of the Eastern Rif (Morocco): magmatic evolution through time. Lithos 45 (1–4), 523–543.

Embey-Isztin, A., Dobosi, G., Bodinier, J.L., Bosch, D., Jenner, G.A., Pourtales, S., Bruguier, O., 2014. Origin and significance of poikilitic and mosaic peridotite xenoliths in the western Pannonian Basin: geochemical and petrological evidences. Contrib. Mineral. Petrol. 168 (3), 1054.

Embey-Isztin, A., Scharbert, H.G., Dietrich, H., Poultidis, H., 1990. Mafic granulites and clinopyroxenite xenoliths from the Transdanubian Volcanic Region (Hungary): implications for the deep structure of the Pannonian Basin. Mineral. Mag. 54 (376), 463–483.

Falus, G., Szabó, C., Vaselli, O., 2000. Mantle upwelling within the Pannonian Basin: evidence from xenolith lithology and mineral chemistry. Terra Nova 12 (6), 295–302.

Faul, U.H., 2001. Melt retention and segregation beneath mid-ocean ridges. Nature 410 (6831), 920–923.

Ferrari, L., 2004. Slab detachment control on mafic volcanic pulse and mantle heterogeneity in central Mexico. Geology 32 (1), 77–80.

Fitton, J.G., James, D., Leeman, W.P., 1991. Basic magmatism associated with late Cenozoic extension in the western United States: compositional variations in space and time. J. Geophys. Res., Solid Earth 96 (B8), 13693–13711.

Fodor, L., Bada, G., Csillag, G., Horváth, E., Ruszkiczay-Rüdiger, Z., Palotás, K., Sikhegyi, F., Timar, G., Cloetingh, S., Horváth, F., 2005. An outline of neotectonic structures and morphotectonics of the western and central Pannonian Basin. Tectonophysics 410 (1–4), 15–41.

Gerya, T.V., Burg, J.-P., 2007. Intrusion of ultramafic magmatic bodies into the continental crust: numerical simulation. Phys. Earth Planet. Inter. 160, 124–142.

Gerya, T.V., Stern, R.J., Baes, M., Sobolev, S.V., Whattam, S.A., 2015. Plate tectonics on the Earth triggered by plume-induced subduction initiation. Nature 527 (7577), 221–225.

Gleason, G.C., Tullis, J., 1995. A flow law for dislocation creep of quartz aggregates determined with the molten salt cell. Tectonophysics 247 (1–4), 1–23.

Harangi, S., 2001. Neogene to Quaternary volcanism of the Carpathian-Pannonian Region – a review. Acta Geol. Hung. 44 (2), 223–258.

Harangi, S., Jankovics, M.É., Sági, T., Kiss, B., Lukács, R., Soós, I., 2015. Origin and geodynamic relationships of the Late Miocene to Quaternary alkaline basalt volcanism in the Pannonian basin, eastern-central Europe. Int. J. Earth Sci. 104 (8), 2007–2032.

Hetényi, G., Ren, Y., Dando, B., Stuart, G.W., Hegedűs, E., Kovács, A.C., Houseman, G.A., 2015. Crustal structure of the Pannonian basin: the AlCaPa and Tisza Terrains and the Mid-Hungarian zone. Tectonophysics 646, 106–116.

Hirth, G., Kohlstedt, D., 2003. Rheology of the upper mantle and the mantle wedge: a view from the experimentalists. In: American Geophysical Union. In: Geophysical Monograph Series, vol. 138, pp. 83–106.

Horváth, F., Bada, G., Szafián, P., Tari, G., Ádám, A., Cloetingh, S., 2006. Formation and deformation of the Pannonian Basin: constraints from observational data. Mem. Geol. Soc. Lond. 32 (1), 191–206.

Horváth, F., Musitz, B., Balázs, A., Végh, A., Uhrin, A., Nádor, A., Koroknai, B., Pap, N., Tóth, T., Wórum, G., 2015. Evolution of the Pannonian basin and its geothermal resources. Geothermics 53, 328–352.

Huismans, R.S., Beaumont, C., 2003. Symmetric and asymmetric lithospheric extension: relative effects of frictional-plastic and viscous strain softening. J. Geophys. Res., Solid Earth 108 (B10), 2496.

Karátson, D., Timár, G., 2005. Comparative volumetric calculations of two segments of the Carpathian Neogene/Quaternary volcanic chain using SRTM elevation data: implications for erosion and magma output rates (with 4 figures and 1 table). Z. Geomorph. Suppl. 140, 19–35.

Kereszturi, G., Csillag, G., Németh, K., Sebe, K., Balogh, K., Jáger, V., 2010. Volcanic architecture, eruption mechanism and landform evolution of a Plio/Pleistocene intracontinental basaltic polycyclic monogenetic volcano from the Bakony-Balaton Highland Volcanic Field, Hungary. Cent. Eur. J. Geosci. 2 (3), 362–384.

Kohlstedt, D.L., 1992. Role of water and melts on upper mantle viscosity and strength. In: Mantle Flow and Melt Generation at Mid-Ocean Ridges. American Geophysical, Union, Washington DC, pp. 103–121.

Koptev, A., Burov, E., Gerya, T., Le Pourhiet, L., Leroy, S., Calais, E., Jolivet, L., 2018. Plume-induced continental rifting and break-up in ultra-slow extension context: insights from 3D numerical modeling. Tectonophysics 746, 121–137.

Koptev, A., Ehlers, T.A., Nettesheim, M., Whipp, D.M., 2019. Response of a rheologically stratified lithosphere to subduction of an indenter-shaped plate: insights into localized exhumation at orogen syntaxes. Tectonics 38 (6), 1908–1930.

Kovács, I., Falus, G., Stuart, G., Hidas, K., Szabó, C., Flower, M.F.J., Hegedűs, E., Posgay, K., Zilahi-Sebess, L., 2012. Seismic anisotropy and deformation patterns in upper mantle xenoliths from the central Carpathian-Pannonian region: asthenospheric flow as a driving force for Cenozoic extension and extrusion? Tectonophysics 514, 168–179.

Kovács, I., Patkó, L., Liptai, N., Lange, T.P., Taracsák, Z., Cloetingh, S.A.P.L., Török, K., Király, E., Karátson, D., Biró, T., Kiss, J., Pálos, Zs., Aradi, L.E., Falus, Gy., Hidas, K., Berkesi, M., Koptev, A., Novák, A., Szabó, C., 2020. The role of water and compression in the genesis of alkaline basalts: inferences from the Carpathian-Pannonian region. Lithos 354, 105323.

Kovács, I., Szabó, C., 2008. Middle Miocene volcanism in the vicinity of the Middle Hungarian zone: evidence for an inherited enriched mantle source. J. Geodyn. 45 (1), 1–17.

Le Bas, M., Maitre, R.L., Streckeisen, A., Zanettin, B., IUGS Subcommission on the Systematics of Igneous Rocks, 1986. A chemical classification of volcanic rocks based on the total alkali-silica diagram. J. Petrol. 27 (3), 745–750.

Le Maitre, R.W., Streckeisen, A., Zanettin, B., Le Bas, M.J., Bonin, B., Bateman, P. (Eds.), 2005. Igneous Rocks: A Classification and Glossary of Terms: Recommendations of the International Union of Geological Sciences Subcommission on the Systematics of Igneous Rocks. Cambridge University Press, p. 256.

Lenkey, L., Dövényi, P., Horváth, F., Cloetingh, S.A.P.L., 2002. Geothermics of the Pannonian basin and its bearing on the neotectonics. EGU Stephan Mueller Spec. Publ. Ser. 3, 29–40.

Matenco, L., Bertotti, G., Leever, K., Cloetingh, S., Schmid, S.M., Tărăpoancă, M., Dinu, C., 2007. Large-scale deformation in a locked collisional boundary: interplay between subsidence and uplift, intraplate stress, and inherited lithospheric structure in the late stage of the SE Carpathians evolution. Tectonics 26, TC4011.

Matenco, L., Radivojević, D., 2012. On the formation and evolution of the Pannonian Basin: constraints derived from the structure of the junction area between the Carpathians and Dinarides. Tectonics 31, TC6007.

Márquez, A., Oyarzun, R., Doblas, M., Verma, S.P., 1999. Alkalic (ocean-island basalt type) and calc-alkalic volcanism in the Mexican volcanic belt: a case for plume-related magmatism and propagating rifting at an active margin? Geology 27 (1), 51–54.

Nelson, D.R., McCulloch, M.T., Sun, S.S., 1986. The origins of ultrapotassic rocks as inferred from Sr, Nd and Pb isotopes. Geochim. Cosmochim. Acta 50 (2), 231–245.

Pécskay, Z., Lexa, J., Szakács, A., Seghedi, I., Balogh, K., Konecny, V., Zelenka, T., Kovacs, M., Póka, T., Fülöp, A., Márton, E., Panaiotu, C., Cvetković, V., 2006. Geochronology of Neogene magmatism in the Carpathian arc and intra-Carpathian area. Geol. Carpath. 57 (6), 511–530.

Petrescu, L., Borleanu, F., Radulian, M., Ismail-Zadeh, A., Maţenco, L., 2021. Tectonic regimes and stress patterns in the Vrancea Seismic Zone: insights into intermediate-depth earthquake nests in locked collisional settings. Tectonophysics 799, 228688.

Posgay, K., Bodoky, T., Hegedüs, E., Kovácsvölgyi, S., Lenkey, L., Szafián, P., Takács, E., Tímár, Z., Varga, G., 1995. Asthenospheric structure beneath a Neogene basin in southeast Hungary. Tectonophysics 252 (1–4), 467–484.

Schmid, S.M., Fügenschuh, B., Kounov, A., Maţenco, L., Nievergelt, P., Oberhänsli, R., Pleuger, J., Schefer, S., Schuster, R., Tomljenović, B., Ustaszewski, K., Van Hinsbergen, D.J., 2020. Tectonic units of the Alpine collision zone between Eastern Alps and western Turkey. Gondwana Res. 78, 308–374.

Seghedi, I., Downes, H., 2011. Geochemistry and tectonic development of Cenozoic magmatism in the Carpathian-Pannonian region. Gondwana Res. 20 (4), 655–672.

Seghedi, I., Downes, H., Szakács, A., Mason, P.R., Thirlwall, M.F., Roşu, E., Pécskay, Z., Márton, E., Panaiotu, C., 2004. Neogene-Quaternary magmatism and geodynamics in the Carpathian-Pannonian region: a synthesis. Lithos 72 (3–4), 117–146.

Sheth, H.C., Torres-Alvarado, I.S., Verma, S.P., 2002. What is the "calc-alkaline rock series"? Int. Geol. Rev. 44 (8), 686–701.

Sleep, N.H., 2003. Geodynamic implications of xenolith geotherms. Geochem. Geophys. Geosyst. 4 (9), 1079.

Sun, S.S., McDonough, W.F., 1989. Chemical and isotopic systematics of oceanic basalts: implications for mantle composition and processes. Geol. Soc. (Lond.) Spec. Publ. 42 (1), 313–345.

Szakács, A., Pécskay, Z., Gál, Á., 2018. Patterns and trends of time-space evolution of Neogene volcanism in the Carpathian-Pannonian region: a review. Acta Geod. Geophys. 53 (3), 347–367.

Tari, G., Dövényi, P., Dunkl, I., Horváth, F., Lenkey, L., Stefanescu, M., Szafián, P., Tóth, T., 1999. Lithospheric structure of the Pannonian basin derived from seismic, gravity and geothermal data. Geol. Soc. (Lond.) Spec. Publ. 156 (1), 215–250.

Ter Voorde, M., Van Balen, R.T., Bertotti, G., Cloetingh, S.A.P.L., 1998. The influence of a stratified rheology on the flexural response of the lithosphere to (un)loading by extensional faulting. Geophys. J. Int. 134 (3), 721–735.

Tesauro, M., Kaban, M.K., Cloetingh, S.A., 2009. A new thermal and rheological model of the European lithosphere. Tectonophysics 476 (3–4), 478–495.

Tetreault, J.L., Buiter, S.J.H., 2018. The influence of extension rate and crustal rheology on the evolution of passive margins from rifting to break-up. Tectonophysics 746, 155–172.

Tóth, L., Mónus, P., Zsíros, T., Kiszely, M., 2002. Seismicity in the Pannonian Region – earthquake data. EGU Stephan Mueller Spec. Publ. Ser. 3, 9–28.

Török, K., 2012. On the origin and fluid content of some rare crustal xenoliths and their bearing on the structure and evolution of the crust beneath the Bakony-Balaton Highland Volcanic Field (W-Hungary). Int. J. Earth Sci. 101 (6), 1581–1597.

Wilks, K.R., Carter, N.L., 1990. Rheology of some continental lower crustal rocks. Tectonophysics 182 (1–2), 57–77.

Wilson, M., Downes, H., 1991. Tertiary-Quaternary extension-related alkaline magmatism in western and central Europe. J. Petrol. 32 (4), 811–849.